Turbulent Fluxes in the Hurricane Boundary Layer. Part II: Latent Heat Flux

WILLIAM M. DRENNAN AND JUN A. ZHANG

Rosenstiel School of Marine and Atmospheric Science, University of Miami, Miami, Florida

JEFFREY R. FRENCH*

Atmospheric Turbulence and Diffusion Division, NOAA/Air Resources Laboratory, Oak Ridge, Tennessee

CYRIL MCCORMICK

Rosenstiel School of Marine and Atmospheric Science, University of Miami, Miami, Florida

PETER G. BLACK

Hurricane Research Division, NOAA/Atlantic Oceanographic and Meteorological Laboratory, Miami, Florida

(Manuscript received 9 March 2006, in final form 20 July 2006)

ABSTRACT

As part of the recent ONR-sponsored Coupled Boundary Layer Air–Sea Transfer (CBLAST) Departmental Research Initiative, an aircraft was instrumented to carry out direct turbulent flux measurements in the high wind boundary layer of a hurricane. During the 2003 field season flux measurements were made during Hurricanes Fabian and Isabel. Here the first direct measurements of latent heat fluxes measured in the hurricane boundary layer are reported. The previous wind speed range for humidity fluxes and Dalton numbers has been extended by over 50%. Up to 30 m s^{-1}, the highest 10-m winds measured, the Dalton number is not significantly different from the Humidity Exchange over the Sea (HEXOS) result, with no evidence of an increase with wind speed.

1. Introduction

Hurricanes are one of the most impressive manifestations of air–sea interaction. Tropical storms derive their energy from latent heat release in the eyewall and return some of it back to the sea through drag on the sea surface. Hence storm modeling, whether using a simple diagnostic approach (Emanuel 1986, 1995) or a fully coupled dynamical one (Chen et al. 2007), requires accurate knowledge of the air–sea fluxes. Air–sea fluxes, however, being relatively difficult to measure, are rarely available outside of a few dedicated campaigns. Consequently, models rely on parameterizations of the fluxes in terms of more readily available parameters.

Typically the fluxes are given in terms of bulk coefficients. For instance the momentum flux, given by

$$\boldsymbol{\tau} = -\rho(\overline{u'w'}\mathbf{i} + \overline{v'w'}\mathbf{j}), \tag{1}$$

is parameterized in terms of the mean neutrally stable 10-m wind speed U_{10N} via the drag coefficient C_D as: $|\boldsymbol{\tau}| = \rho C_D U_{10N}^2$. Here ρ is the air density, u', v', and w' are the turbulent components of horizontal in-line (with the mean wind), horizontal crosswind and vertical velocities, respectively, and the overbar refers to time averaging over a suitable period. We assume the mean surface current to be negligible with respect to U_{10N}. For future reference we define the friction velocity $u_* = (|\boldsymbol{\tau}/\rho|)^{1/2}$. Similarly the bulk humidity flux coefficient or Dalton number is given by

$$C_E = \overline{q'w'}/[U_{10N}(Q_0 - Q_{10N})]. \tag{2}$$

* Current affiliation: Department of Atmospheric Sciences, University of Wyoming, Laramie, Wyoming.

Corresponding author address: Dr. William M. Drennan, Rosenstiel School of Marine and Atmospheric Science, University of Miami, 4600 Rickenbacker Causeway, Miami, FL 33149.
E-mail: wdrennan@rsmas.miami.edu

DOI: 10.1175/JAS3889.1

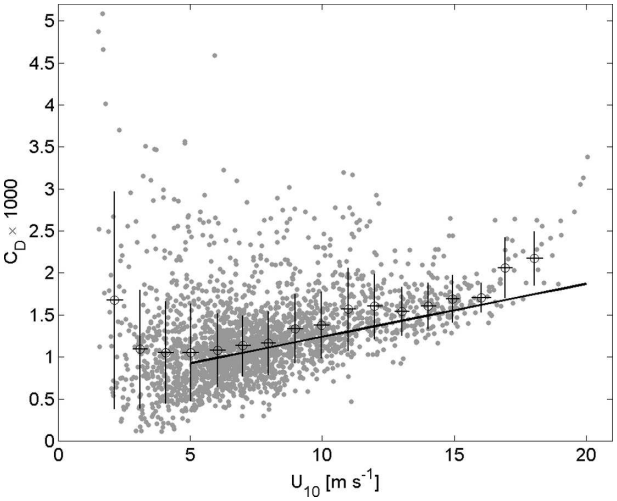

FIG. 1. Plot of drag coefficient vs wind speed at 10-m height for neutral stability, from eight field experiments. The experiments, all using the eddy-correlation method for measuring fluxes, are listed in the text. The curve is from Smith (1980). The circles and thin lines show the mean and 1 standard deviation of the data in bins of 1 m s^{-1}.

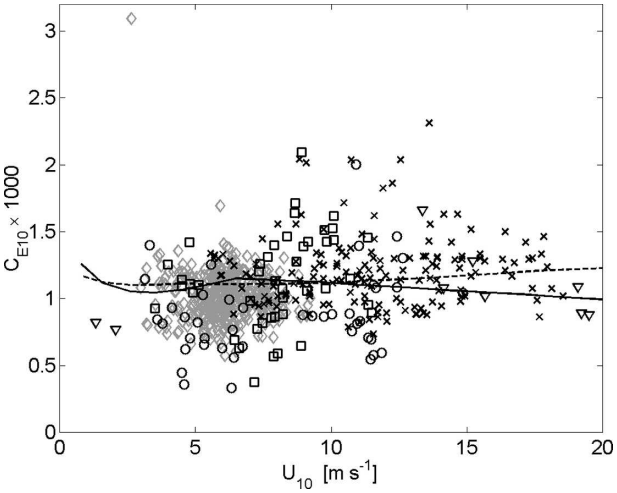

FIG. 2. Plot of Dalton number vs wind speed at 10-m height for neutral stability, from five field experiments. The experiments, all using the eddy-correlation method for measuring fluxes, are AGILE (○: Donelan and Drennan 1995), HEXOS (×: DeCosmo et al. 1996), GASEX (◇: McGillis et al. 2004), SOWEX (▽: Banner et al. 1999), and SWADE (□: Katsaros et al. 1993). Data have been corrected for density variations (Webb correction) and (as necessary) for salinity effects. The curves are from Fairall et al. (1996, solid), and Fairall et al. (2003, dashed).

Here q' is the turbulent specific humidity, and Q_{10N} and Q_0 are the neutral 10 m and surface mean specific humidities, respectively.

After three decades of air–sea turbulence flux measurements, there is a general consensus on the behavior of the parameterizations of momentum, humidity, and heat fluxes at moderate wind speeds. The drag coefficients shown in Fig. 1, an ensemble from eight field experiments, are typical of most recent campaigns. The experiments are from the small ship R/V *Agile* in Lake Ontario (Donelan and Drennan 1995); Adverse Weather Experiment (AWE), from an Air–Sea Interaction Spar (ASIS) buoy off the Florida coast (Drennan and Shay 2006); flux, état de la mer, et télédétection en conditions de fetch variable (FETCH), from an ASIS buoy in the Mediterranean Sea (Drennan et al. 2003); The Equatorial Pacific Air–Sea CO_2 Exchange Experiment (GASEX), from an ASIS buoy (McGillis et al. 2004); HEXOS, from a tower in the North Sea (Smith et al. 1992; Janssen 1997); Risø Air–Sea Exchange (RASEX), from a tower in the Baltic Sea (Johnson et al. 1998); Surface Wave Dynamics Experiment (SWADE), from a ship in the coastal Atlantic (Donelan et al. 1997), and Water–Air Vertical Exchange Study (WAVES), from a tower in Lake Ontario (Drennan et al. 1999).

For wind speeds between 4 and 20 m s^{-1}, C_D increases roughly linearly with wind speed. The classic curve of Smith (1980) is shown on Fig. 1. Additional variability in C_D is due to wave age (Kitaigorodskii and Volkov 1965; Drennan et al. 2003) and swell (Volkov 1970; Donelan et al. 1997). The effect of wave age is to increase the drag in fetch- or duration-limited conditions. Most of the data points lying well above the Smith curve in Fig. 1 represent fetch-limited conditions, while the Smith curve itself is typical of fully developed seas (Drennan et al. 2003). Swell can either decrease or increase C_D depending on whether the swell waves are propagating with or against the wind (Drennan et al. 1999).

Humidity flux data are less numerous than those of momentum flux due to the lack (until recently) of fast response hygrometers suitable for the marine environment. Dalton numbers from five field experiments are shown in Fig. 2. The experiments, representing a wide range of conditions, are AGILE, GASEX, HEXOS (DeCosmo et al. 1996), Southern Ocean Waves Experiment (SOWEX; Banner et al. 1999), and SWADE (Katsaros et al. 1993). All flux data were calculated via eddy correlation with mean wind speeds and humidity corrected to neutral stratification. The 168 HEXOS points, which were extracted from Fig. 6a of DeCosmo et al., include data from both HEXOS systems. Following Fairall et al. (2003), we increase the measured HEXOS values by 8% (see below). Although the datasets exhibit considerable scatter, there is no significant dependence of Dalton number with wind speed. This is consistent with most earlier results, such as Large and Pond (1982).

Several theoretical studies of humidity transfer based

on surface renewal theory have been carried out. The models typically consider roughness lengths instead of bulk coefficients. These roughness lengths z_{0i} are the heights above the surface where the (assumed) logarithmic profiles of mean wind speed, humidity, etc., reach their surface values. The neutral bulk coefficients and z_{0i} are related as

$$C_D = \kappa^2[\log(10/z_{0u})]^{-2} \quad (3)$$

$$C_E = \kappa^2[\mathrm{Pr}\log(10/z_{0q})\log(10/z_{0u})]^{-1}, \quad (4)$$

where z_{0u} and z_{0q} are the respective roughness lengths for momentum and humidity, and $\kappa \approx 0.4$ is the von Kármán constant. Following Donelan (1990), we assume a Prandtl number, Pr = 0.85. Generally z_{0q} is taken as a function of the roughness Reynolds number, $\mathrm{Re} = z_{0u}u_*/\nu$, where ν is the kinematic viscosity.

The Liu et al. (1979) model, updated and enhanced by Fairall et al. (1996) as COARE-2.5, predicts the Dalton number to decrease with increasing wind speed, as increased sheltering behind the higher roughness elements increases the local time for renewal of the surface by the bulk fluid. The COARE-2.5 curve is given in Fig. 2. The use of alternate functional forms for $z_{0q} = f(\mathrm{Re})$ in the models leads to C_E being roughly constant (Brutsaert 1975) or increasing somewhat with wind speed (Zeng et al. 1998). The COARE-3 curve of Fairall et al. (2003), also shown on Fig. 2, represents the current state of the art. COARE-3 is based on over 2700 h of eddy covariance data, including 160-h with wind speeds exceeding 10 m s^{-1}. Given that 94 h of these higher wind data are from HEXOS, it is not surprising the COARE-3 curve represents a good fit to the HEXOS data. However, with the high degree of scatter in the data, especially at high wind, it is not clear that either curve can be favored over a simple constant coefficient.

Figures 1 and 2 are typical of existing flux datasets in that there are very few direct air–sea flux measurements for wind speeds over 22 m s^{-1}. To the authors' knowledge, there are no humidity flux measurements above 20 m s^{-1}. Hence the use of bulk relations in higher wind conditions requires extrapolating them well beyond their validated range and into a regime where enhanced wave breaking, sea spray, and bubbles may dramatically change the transfer processes (see below).

This approach has been called into question by the modeling work of Emanuel (1986, 1995). Emanuel, using a simple axisymmetric hurricane model, finds that the maximum predicted wind speed is proportional to the ratio of the bulk coefficients of moist enthalpy and momentum, C_K/C_D. Here moist enthalpy $k = [c_p(1 - q) + c_l q]T + L_v q$, where T is the air temperature, c_p and c_l the specific heats of air (at constant pressure) and liquid water, respectively, and L_v is the latent heat of vaporization. Assuming the bulk humidity and sensible heat coefficients to be equal, as is typical for wind speeds under 20 m s^{-1}, C_K can taken to be equal to C_E. Based on the comparison of model predictions with observations, Emanuel finds the most likely range of the C_K/C_D ratio is 1.2 to 1.5, with a lowest bound of 0.75. For $C_K/C_D < 0.75$ the energy lost to drag exceeds that gained from enthalpy, and tropical storms die down. However as can be determined from Figs. 1 and 2, $C_E/C_D \approx 0.5$ for $U = 20$, and decreases as the coefficients are extrapolated to higher winds. Hence if existing bulk flux relations are used in a model, hurricanes will not develop.

We point out that the present (until 2007) operational hurricane model of the National Oceanic and Atmospheric Administration (NOAA) (Kurihara and Tuleya 1974; Kurihara et al. 1998) uses a bulk flux algorithm with a single roughness; that is, $z_{0q} = z_{0u}$. This results in $C_E = C_D$. Although this approach represented early thinking on the matter (e.g., Zhang and Anthes 1982), it is clearly not supported by recent data (Figs. 1 and 2). It does however meet the Emanuel criterion, which perhaps explains its continued use in some models.

Over the past few years, considerable attention has been focused on increasing our understanding of high wind air–sea interaction processes. Powell et al. (2003) and Donelan et al. (2004) have recently shown, using roughness inferred from extrapolated GPS dropsonde profiles and laboratory measurements, respectively, that the drag coefficient levels off at wind speeds over 30–40 m s^{-1}. Nevertheless, even with the leveling-off of the drag, the Emanuel criterion cannot be met without a commensurate increase in Dalton number, perhaps due to sea spray (Andreas and DeCosmo 2002). There remains the need for flux measurements in the high wind regime.

We report here the first direct measurements of humidity flux in the high wind regime. These data, from the boundary layers of 2003 Hurricanes Fabian and Isabel, were collected during the ONR-sponsored Coupled Boundary Layer Air–Sea Transfer (CBLAST) hurricane experiment. Henceforth we use CBLAST to refer only to the hurricane component of the larger CBLAST departmental research initiative. One of the long-term CBLAST objectives, as well as a key goal of NOAA's Environmental Modeling Center, is to improve model predictions of both hurricane intensity and track. An improved understanding of air–sea fluxes at high winds is viewed as essential to achieving these goals. We provide a brief summary of the CBLAST

experiment (section 2), with detailed description of the aircraft sensors used here (section 3). The data analysis is presented in section 4, followed by the results and discussion in sections 5 and 6.

2. The CBLAST experiment

The CBLAST experiment, described in detail by Black et al. (2007), took place in the Atlantic during the 2002–04 hurricane seasons. CBLAST was designed as a multiplatform experiment, using several aircraft and a variety of sondes and buoys to probe the hurricane and surrounding atmosphere and ocean. The focus of this paper is on measurements of the turbulent flux of latent heat in the hurricane boundary layer. These measurements were carried out from "Hurricane Hunter" N43RF, one of two Orion WP-3D research aircraft operated by NOAA's Aircraft Operation Center (AOC).

A typical flight pattern of N43RF is shown in Fig. 3. The example shown is for the 14 September 2003 flight into Hurricane Isabel. On that day, Isabel was a strong Category 4 hurricane, with maximum sustained surface winds around 72 m s^{-1} (140 kt). The aircraft took off from St. Croix, U.S. Virgin Islands, at 1450 UTC (1050 LT). The 8-h flight included an initial calibration of the gust probe sensors (denoted A on Fig. 3), an eyewall penetration (B) at 3700 m, and several stepped descents into the boundary layer (C). The descents were carried out in clear regions between rainbands. After an initial descent (C1) was aborted due to poor visibility, along-wind and across-wind descents were made at C2, and an along-wind descent at C3. Each stepped descent consisted of a series of roughly 30-km legs at nominal heights of 600, 400, 200, 120, and 60 m (Fig. 3). During many descents, the lowest altitude reached was only about 100 m owing to the presence of clouds or rain.

In total, six flux flights were made during the 2003 season. On 2, 3, and 4 September flights were made into Hurricane Fabian, then a major hurricane north of the Antilles moving from 20°N, 60°W on 2 September to 25°N, 64°W on 4 September. Three additional flights were conducted into Hurricane Isabel on 12, 13, and 14 September. At this time Isabel was a Category 4–5 storm following a path similar to that of Fabian (tracking 22°N, 57°W to 24°N, 67°W). Most stepped descents were made between 100 and 150 km from the storm center. During three days, flux runs were conducted in the right rear quadrant (with respect to storm motion). Two days were spent in the right front quadrant, and one day in the left front. Although the intention had been to sample in all four quadrants in order to cover the full range of wave conditions, this was not achieved.

Flights of N43RF were coordinated with those of a second NOAA P3, N42RF. During N43RFs low-level stepped descents, N42RF would fly above N43RF releasing GPS dropsondes (Powell et al. 2003) to measure boundary layer characteristics. An example of the GPS profile data of wind speed, humidity, and potential temperature Θ is given in Fig. 4. Boundary layer (BL) depths were estimated from the Θ profiles to be around 500 m in the vicinity of the flux measurements. This is consistent with estimates derived using Anthes and Chang (1978) and Kepert (2001). Only data collected within the BL are used in this study.

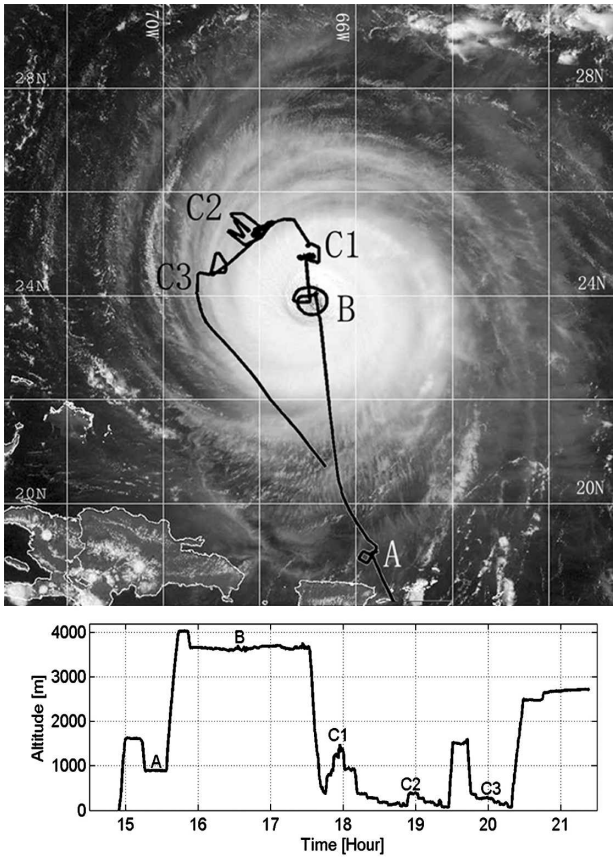

FIG. 3. Track of N43RF into Hurricane Isabel on 14 September 2003. The highlighted features are A: gust probe calibration, B: eye penetration, and C: stepped descents. The visible band image, from the NOAA Geostationary Operational Environmental Satellite *GOES-12* at 1745 UTC, is coincident with B. Image is courtesy of Naval Research Laboratory, Monterey, CA. (bottom) Plot of aircraft elevation vs time for above flight.

The aircraft sensors used here are described below and in a companion paper (French et al. 2007). Here we focus on the instrumentation and methods used to measure humidity and humidity flux.

3. Aircraft sensors and data analysis

One issue addressed early in the CBLAST campaign was the need for a fast response hygrometer for use on

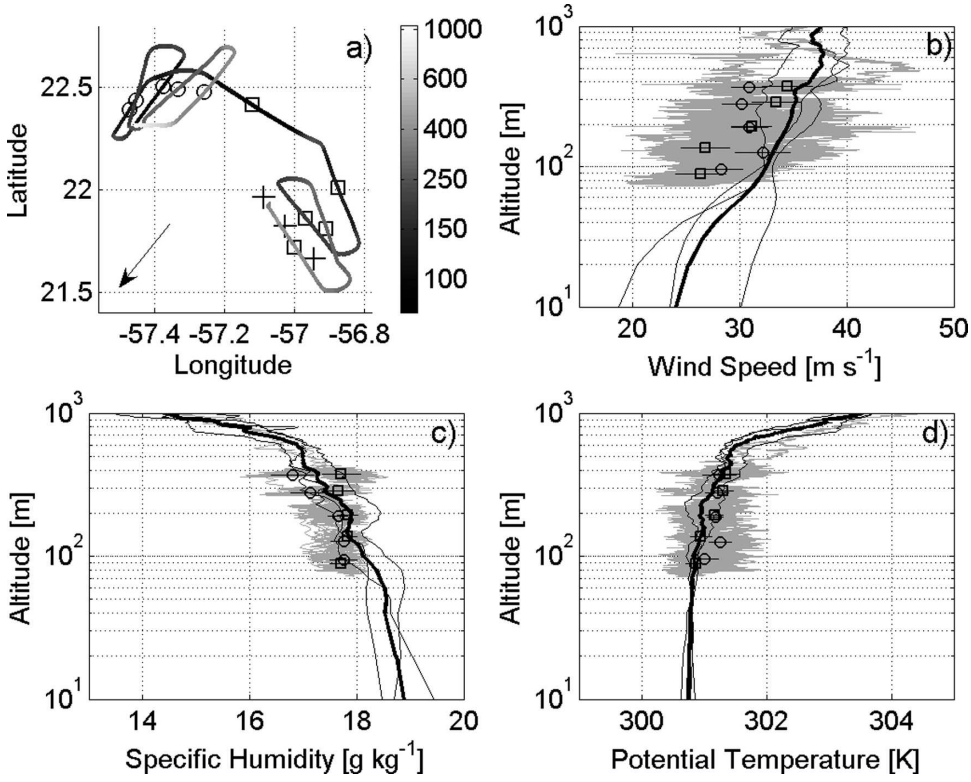

FIG. 4. Profiles of (b) wind speed, (c) specific humidity, and (d) potential temperature during stepped descents into Hurricane Isabel on 12 Sep 2003. The gray lines are measurements from N43RF (a) during the stepped descents. The boxes and circles represent the means of along- and crosswind flux runs, respectively, with the horizontal bars representing 1 standard deviation. The thin lines are data from the three GPS dropsondes released from N42RF at the pluses in (a). The thick line is the mean of the sondes. In (a), the arrow points to the direction of the eye, while the grayscale denotes altitude.

the P3 aircraft. During the Tropical Ocean Global Atmosphere Coupled Ocean–Atmosphere Response Experiment (TOGA COARE) in 1992–93, when turbulent fluxes were measured from both P3s, suitable humidity measurements were made using Lyman-α hygrometers (Khelif et al. 1999). Unfortunately, the Lyman-α's are no longer serviceable, and were therefore unavailable for CBLAST. Most fast response humidity measurements today are made with infrared gas analyzers (IRGA). As closed path IRGAs lose calibration when liquid water enters the sampling chamber, they were not deemed suitable in the rain- and spray-filled environment of a hurricane. Open path IRGAs such as the LI-COR LI-7500 do not suffer this problem, but they are neither designed nor recommended for deployment on aircraft (D. Anderson 2003, LI-COR Inc., personal communication). In particular, the thin struts that support the instrument head are prone to vibration, which can affect the measurement. The struts could also fail, possibly resulting in damage to the aircraft.

Our approach for CBLAST was to mount a LI-7500 in an aluminum enclosure (Fig. 5), with the instrument head strapped down. The box was mounted in the radome, directly behind the turbulence gust probes, which are used to measure the turbulent velocity fluctuations. Airflow to the LI-7500 was provided via a Rosemount 102E4 housing (Goodrich Sensors) with a Buck Research IP-100 intake, and 70 cm long by 2-mm dia Teflon tubing. A low-density polyethylene (LDPE) insert with a 1.5-cm bore and ports near each end was mounted in the LI-7500 head to direct the airflow. A third port was connected to an Omegadyne PX-02K1 barometer allowing for the measurement of pressure within the chamber. The insert is similar in principal to the calibration tube provided by LI-COR, but is able to be secured in place against vibration.

The aluminum enclosure, which also housed the LI-7500 electronics, was insulated (Orcotek 09–45015) and maintained at a constant 40°C temperature with two Minco Kapton HK-5177R58.8L12A thermofoil heaters, a Sunon SF11580 fan, and a Minco CT325PF2B5 controller. A Systron Donner BEI MotionPak was installed in the enclosure to measure all six components

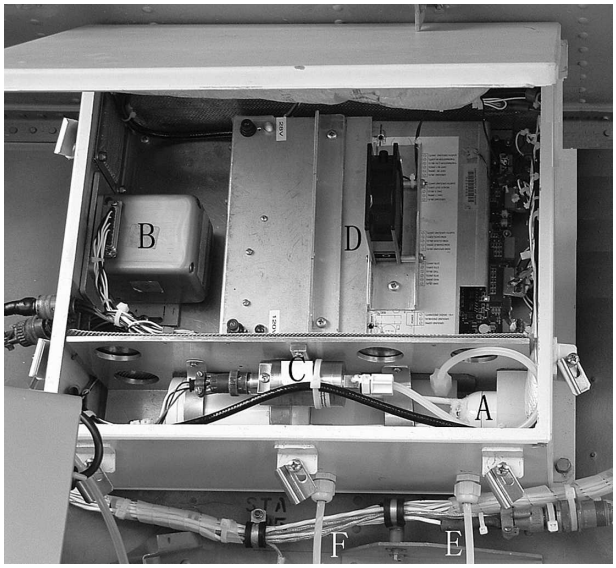

FIG. 5. Photograph of hygrometer box mounted on P3. The highlighted components are A: LI-7500 head, B: MotionPak, C: barometer, D: fan, E: intake, and F: exhaust.

of aircraft motion (three linear accelerations, and three angular rates) in the nose. Both 120 V ac and 28 V dc power were provided to the enclosure. All channels from the enclosure (hygrometer, motion, and pressure) were sampled at 40 Hz using the aircraft data acquisition system installed for TOGA COARE. With typical airspeeds of 113 m s^{-1}, this corresponds to a sampling interval of 2.8 m.

The LI-7500 was calibrated in its enclosure in the hangar or in the laboratory both pre- and postfield season using a LI-COR LI-610 dewpoint generator. During each flight, the calibration was checked against the humidity calculated from a slow-response thermistor and chilled-mirror hygrometer (General Eastern 1011) located along the fuselage aft of the cockpit and sampled at 1 Hz. In Fig. 6a, we show a comparison of the two humidity signals during the first two minutes of a typical flux run (from 1923:28 UTC 14 September 2003). Here the latter signal has been advanced by 2.5 s to account for both the slower instrument response and downwind position of the chilled mirror. The 2.5 s was determined from the phase lag between the two signals.

Figure 6b shows the comparison of the 1-s LI-7500 and slow aircraft absolute humidity during the full 7-h flight of 14 September 2003. There was little evidence of sea spray or rain affecting the LI-COR signal, despite the passage of the aircraft through regions of heavy rain: the Rosemount housing appears to be performing according to design by excluding most droplets. The correlation between the two signals during the flight is $\gamma^2 = 0.993$; the best-fit linear regression between the two, $q_{\text{dew}} = 0.958q_{\text{LI}} + 0.467$, is not significantly different from the 1:1 line. Neither the regression nor the correlation coefficient changed significantly during the six CBLAST flight days. Figure 6c shows a comparison of the two humidity spectra during the flux run of Fig. 6a. It is evident that the two signals agree well at frequencies lower than 0.3 Hz. At higher frequencies, the LI-7500 q' spectrum shows a well-defined inertial subrange, while the slow aircraft system spectrum rolls off.

The wind vector was measured using three systems: a five-hole gust probe system on the radome (Khelif et al. 1999), Rosemount five-hole 858Y probes with Rosemount 1221F1VL transducers on the fuselage, and the nine-hole Best Aircraft Turbulence (BAT: French et al. 2007) gust probe system installed at the end of a 2-m boom in front of the nose. The velocity data were corrected for aircraft motion measured using the onboard Inertial Navigation System (Northrop/Delco Carousel-IV) and GPS. As discussed above, aircraft motion was also measured using a BEI MotionPak in the radome. However, as one of the channels in the MotionPak failed, the sensor was not used in the analysis. Details of the velocity sensors and motion correction, including a comparison of the derived vertical velocities, are presented in the companion paper (French et al. 2007). As one of the radome differential pressure sensors failed during CBLAST, data presented here are from the BAT or Rosemount sensors. During the flights into Hurricane Fabian, the BAT probe was not operational. During those days the vertical velocity was calculated from the Rosemount attack, sideslip, and static pressure sensors on the fuselage along with the radome total temperature sensor.

In Fig. 7, we show $q'w'$ cospectra from the same run as Fig. 6, a time when both BAT and Rosemount systems were functioning. The figure shows the cospectra of q' with each of the BAT and Rosemount vertical velocities. Here time lags of $\varsigma = 0.2$ s and $\varsigma_R = \varsigma + 0.1 = 0.3$ s have been applied to the BAT and Rosemount w', respectively, before correlation with the LI-COR q'. The agreement between the two systems is seen to be very good at all frequencies. In Fig. 8 we plot a comparison of the $\overline{q'w'}$ covariances calculated using the BAT probe w' with those calculated using the vertical velocity from the Rosemount sensors. These data are from Hurricane Isabel when both gust probe systems were operating. The correlation between the two estimates is $\gamma^2 = 0.94$, and the maximum likelihood regression gives $\overline{q'w'}_{\text{BAT}} = 1.17\overline{q'w'}_{\text{Rose}} - 0.02$. The scatter between the two estimates is typical of similar comparisons and does not indicate a significant differ-

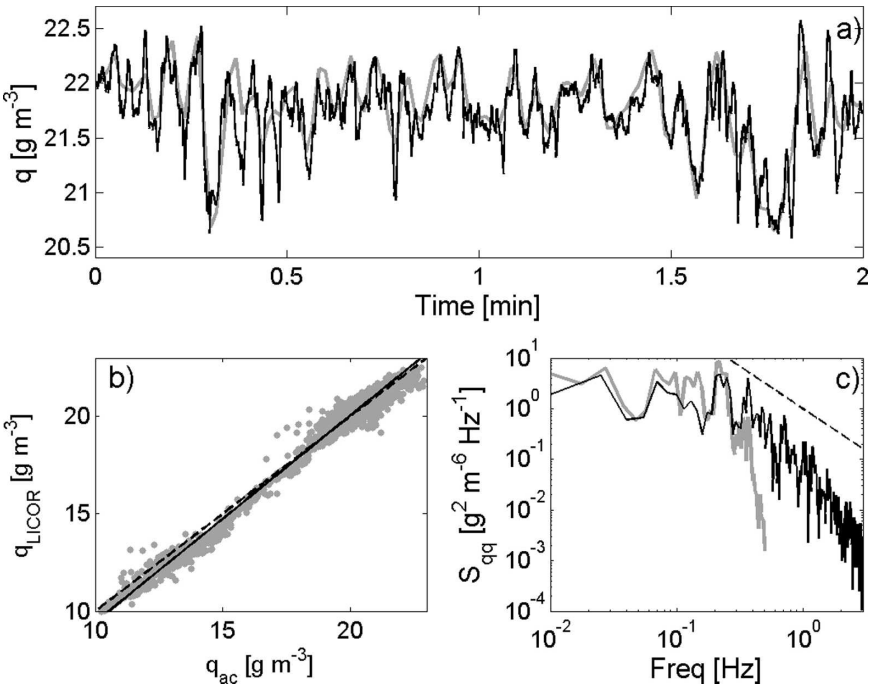

FIG. 6. Comparison of absolute humidity from the LI-7500 (black lines) and slow response aircraft thermistor and chilled-mirror hygrometer system (gray lines). (a) Two-minute time series comparison from 1923:28 UTC 14 Sep 2003. (b) Scatterplot of the 1-s data for the entire 7-h flight of 14 September; the dashed and solid lines are the best fit regression and 1:1 lines, respectively. (c) Frequency spectra from the flux run of (a); the dashed line shows the expected inertial subrange slope.

ence between the two systems. Consequently, we treat the data from the two systems equally, although flow distortion and upwash effects are expected to be lower with the BAT.

4. Humidity flux

During the stepped descents, periods were identified where conditions were relatively stationary and the aircraft motion changes minimal. In particular, the aircraft

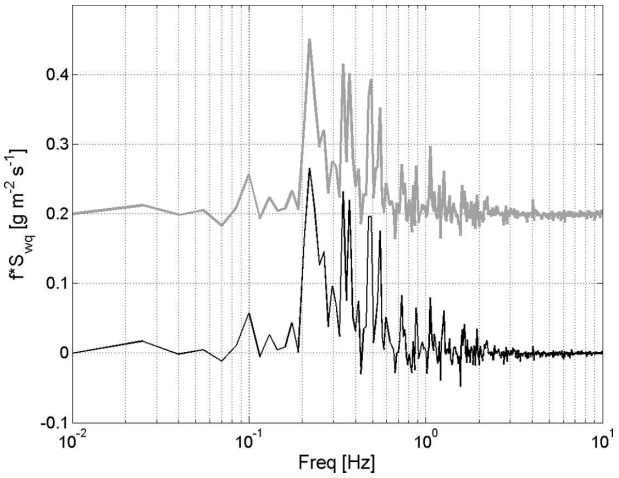

FIG. 7. Cospectra of LI-7500 absolute humidity with vertical velocity calculated from the BAT (black line) and Rosemount (gray line, offset by 0.2) systems. The data are from 1922:27–1925:47 UTC 14 Sep 2003. True airspeed is 113 m s^{-1}.

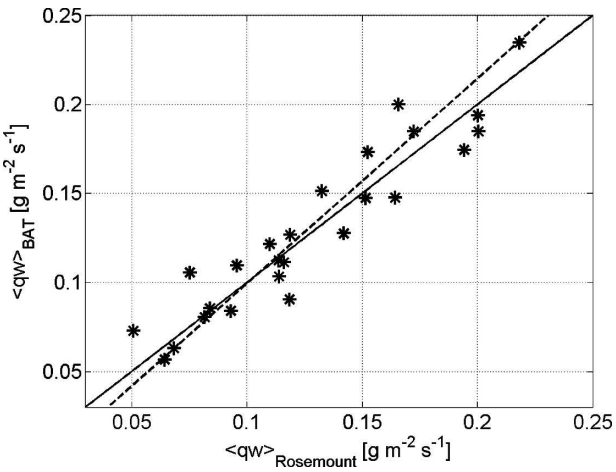

FIG. 8. Comparison of covariances $\langle qw \rangle$ of LI-7500 absolute humidity with vertical velocity calculated from the BAT and Rosemount systems. The dashed and solid lines are the best-fit regression and 1:1 lines, respectively.

pitch, roll, and heading, along with the altitude, the three velocity components and the humidity were inspected. Often only a smaller segment of a given run was suitable for analysis. For these periods spectra and cospectra were calculated. Cumulative fluxes and ogives were also calculated and used to classify the fluxes. Bad runs (those with dominant low-frequency contributions or open ogives—see French et al. 2007) were flagged as likely undersampled, often due to dominant gusts or boundary layer rolls (Foster 2005). These runs are not included in the present analysis, but will be investigated as part of a separate study.

A total of 42 suitable BL flux runs from the six flights were made. The data are summarized in Table 1 of French et al. (2007). Note that six of the runs used for momentum flux calculations were not deemed suitable for humidity flux calculations. As the LI-7500 measures water vapor density or absolute humidity (ρq), and not specific humidity q as required by (2), we apply the Webb et al. (1980) correction as described by Fairall et al. (2003). This correction increases the measured fluxes by about 3%. Although the humidity flux is measured at order 100 m above sea level, the quantity of interest is the surface flux. In Fig. 9 we show profiles of $\overline{q'w'}$ in the boundary layer where each profile represents a stepped descent. Only profiles with four or more points are used. A statistical analysis of the profile slopes indicates the CBLAST data to be constant with height (95% confidence), in support of the DeCosmo et al. (1996) HEXOS aircraft data, as well as those of Nicholls and Readings (1979). We therefore take the measured fluxes as indicative of surface values.

Although the surface fluxes are the physical quantity of interest, as discussed above models typically rely on bulk parameterizations, with 10 m chosen as the standard reference height. To calculate the neutral 10-m Dalton number, in addition to the surface fluxes, the bulk mean humidity difference $Q_0 - Q_{10N}$ and mean wind speed U_{10N} are needed. Below we provide estimates of these quantities, although the meaning of 10-m wind speeds and humidities is unclear in an environment where individual wave heights reach 20 m (Wright et al. 2001).

We calculate the surface humidity Q_0 from the sea surface temperature, assuming saturation and making a 2% reduction to account for salinity effects. Sea surface temperature was measured from the P3s using a Barnes PRT-5 (precision radiation thermometer) radiometer. The PRT-5 operates in the narrow infrared band 9.5–11 μm. Its absolute accuracy is stated by the manufacturer to be ± 0.5°C. The radiometer temperature T_{IR} is affected not only by radiation emitted by the sea surface (i.e., by sea surface temperature), but also by sky radiation reflected from the sea surface and by absorption and reradiation by the intervening atmosphere. Plots of measured infrared temperature versus altitude during stepped descents show a roughly linear trend in the BL (Fig. 10). Although the mean slope is close to that of Burns et al. (2000), -0.0017 K m^{-1}, it was found to vary according to SST, even changing signs for the first descent of 12 September 2003, when SST was only 26.2°C (Fig. 10a). Here we use a different linear correction for each stepped descent. A correction for sky reflection (Burns et al. 2000) is not made here, as the longwave radiation was not measured on the aircraft. We note that the cooler SSTs seen on 12 September 2003 (as well as 2 and 13 September) were measured in the right rear storm quadrants. These are evidence of the cool wake following a hurricane, the result of the strong ocean mixing induced by the hurricane winds (Black et al. 2007).

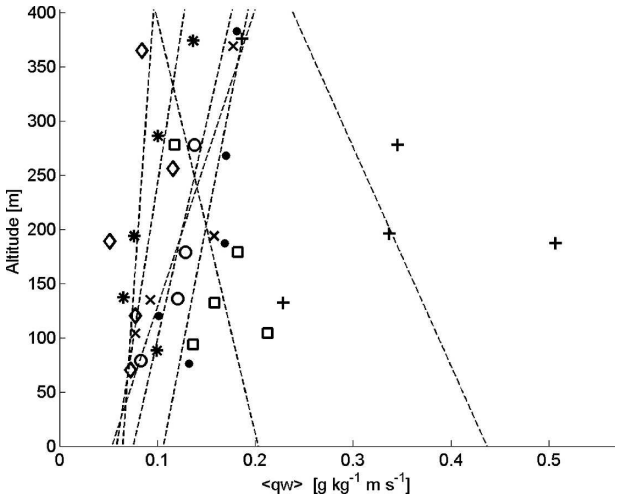

FIG. 9. Plot of $\langle qw \rangle$, covariance of specific humidity with vertical velocity, vs altitude z for CBLAST stepped descents. Only descents with four or more altitudes are used. Symbols representing the different descents in September are ○: 02, +: 03, ×: 04, *: 12, ◇: 13, □: 14-1, ●: 14-2; dashed lines represent slopes for each descent.

In calculating Q_{10N}, we correct the measured mean flight level humidity Q_z to neutral stability, then extrapolate to 10 m by assuming a logarithmic profile:

$$Q_Z - Q_O = \mathrm{Pr} q_* \kappa^{-1} [\log(z/z_{0q}) - \Psi_q(z/L)]. \quad (5)$$

Here $q_* = -\overline{q'w'}/u_*$, and we use the profile function $\Psi_q(z/L)$ of Donelan (1990) to convert the data to neutral stability. The Obukhov length L is calculated from the mean flight-level parameters using an iterative algorithm. Although the assumption of a logarithmic mean profile in Q may be questionable in the hurricane

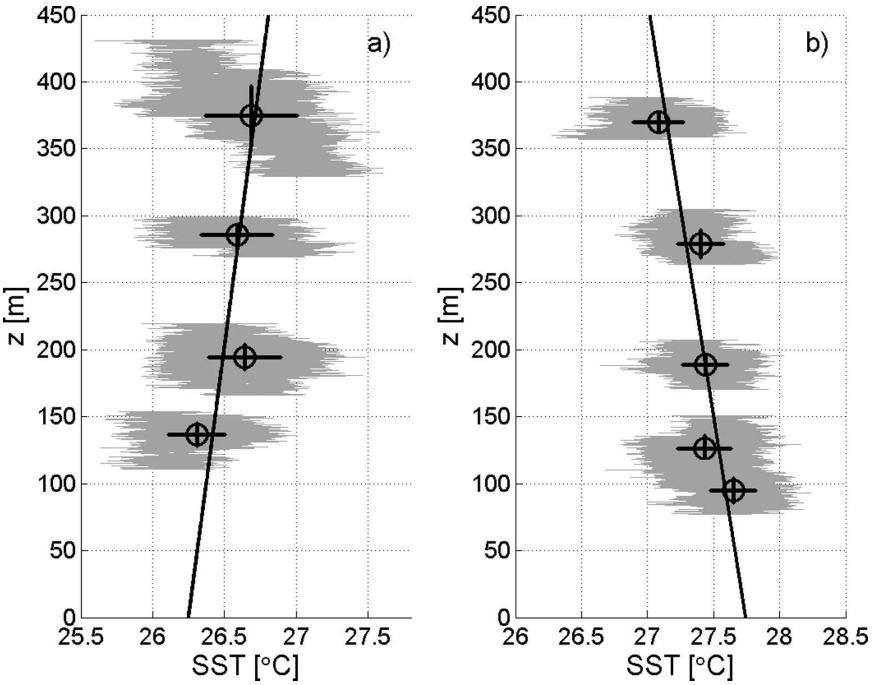

FIG. 10. Plot of radiometric sea surface temperature vs altitude for two stepped descents on 12 September.

boundary layer, there is support from both the stepped descents and GPS sonde profiles. See, for instance, Fig. 4c from 12 September 2003. Here the mean of the three sonde profiles has a shape similar to the profile formed from the mean Q values of the stepped descents: each is near logarithmic. The offset in humidity between the GPS and descent profiles is likely accounted for by the spatial offset between the two. The stability correction in (5) is small: it increases Q_{10N} by a mean of 1% and decreases Q_0–Q_{10N} by a mean of 3%.

Several approaches were made in estimating the neutral 10-m wind speed. Efforts to use the stepped descent mean winds extrapolated to the surface proved unsuccessful: owing to inhomogeneities in the storm, a classical logarithmic wind profile was rarely observed during a stepped descent. During one descent, the mean wind increased approaching the surface!

In a second approach, we assume a logarithmic mean wind profile and extrapolate individual flux runs to the 10-m level using the measured friction velocity, u_*:

$$U_z = u_* \kappa^{-1} [\log(z/z_{0u}) - \Psi_u(z/L)]. \quad (6)$$

Here u_* is calculated as per French et al. (2007), and $\Psi_u(z/L)$ is from Donelan (1990). The assumption of a logarithmic profile down to 10 m was made by Powell et al. (2003) in their recent study using GPS dropsondes. Although individual sonde profiles often departed significantly from logarithmic behavior (e.g., Fig. 4b), profiles averaged by relative height (with respect to boundary layer height) and binned by wind speed were found to be logarithmic in the mean.

Finally, near-surface wind speeds are estimated using the stepped frequency microwave radiometer (SFMR: Uhlhorn and Black 2003) on N43RF. The radiometer measures brightness temperature T_B at six microwave frequencies between 4.55 and 7.22 GHz. As the wind speed increases, so does the percentage of foam covering the sea surface. The increasing presence of foam, an effective blackbody, increases the emissivity and therefore T_B with the effect increasing with frequency (in the microwave band). Uhlhorn and Black (2003) present the theory and algorithm used to extract wind speed from T_B. The SFMR wind speed measurements were validated against near-surface (10 m) wind speeds from collocated GPS dropsondes. Here we use the latest SFMR wind speed algorithm, SWEMODv2, developed using data from the 2005 hurricane season (Uhlhorn et al. 2007).

While the profile-derived and SFMR 10-m winds agree well in the mean (no significant difference) at altitudes below 170 m, the profile-derived winds at higher altitudes are 2.1 ± 0.5 m s^{-1} higher in the mean than the SFMR winds, with the profile-derived surface winds showing much higher variability within given

stepped descents than the SFMR surface winds. Here we take the SFMR winds to be the best estimate of U_{10}. This avoids the need to assume logarithmic wind speed profiles, which we consider questionable in these conditions.

5. Dalton number

In Fig. 11 we plot the CBLAST neutral 10-m Dalton numbers versus wind speed. The mean value of the 42 points is $1.18 \pm 0.07 \times 10^{-3}$, showing 1 standard error. This is close to the original HEXOS mean value ($C_E = 1.12 \times 10^{-3}$) and is slightly above the GASEX and SOWEX means. Fairall et al. (2003) revised the HEXOS data by applying the Webb correction, accounting for the 2% reduction in saturated humidity due to salinity, and adjusting for the use of an $O(5\text{ m})$ bulk value for sea surface temperature. The net effect was to raise the original HEXOS Dalton numbers by 8% to $C_E = 1.2 \times 10^{-3}$, slightly (but not significantly at 95%) above the present result.

It is evident from Fig. 11, however, that there is much more scatter or variability in the CBLAST data than the earlier, lower wind datasets. In stationary conditions, the sampling error of a turbulent flux (e.g., $F = \overline{q'w'}$) is often expressed as

$$\sigma_F/\overline{F} = \alpha_F z^{1/2} U^{-1/2} \Upsilon^{-1/2}, \tag{7}$$

where σ_F represents the standard deviation of flux estimates, α_F is a constant, U is the speed of advection of turbulence past the probe (m s^{-1}), Υ is the sampling interval (s), and z the altitude (m) (e.g., Sreenivasan et al. 1978). For $F = \overline{q'w'}$, Sreenivasan et al. estimate $\alpha_F = 6.4$. We assume a similar value of α_F when looking at the variability in C_E.

During GASEX when conditions were largely stationary ($z = 6.5$; $\overline{U} = 6.1$, $\Upsilon = 1800$), the measured variability $\sigma_F/\overline{F} = 0.18$ is well predicted by (7), which gives 0.16. For HEXOS, the measured variability of 0.22 considerably exceeds that predicted (0.10), likely an indication of the varying (i.e., nonstationary) conditions during the 7-week-long HEXOS campaign. The CBLAST measurements were carried out at considerably higher altitudes ($z = 60 - 400$ m), higher relative wind speeds ($\overline{U} \approx 110\ \text{m s}^{-1}$) and shorter durations ($\Upsilon \approx 270$ s) than the surface-based ones. Again using (7), the expected variability in the CBLAST data is 52%—consistent with the measured variability of 38%. Hence, we can conclude that the higher observed variability in the CBLAST data is consistent with the CBLAST sampling.

There is a variety of factors that could lead to systematic bias in the measurements. Considering first the sensors themselves, as discussed above, each compared well with independent aircraft sensors; for example, the LI-COR with the dewpoint hygrometers, the Rosemount and BAT velocities, the motion packages. Furthermore, the algorithms were coded and run largely independently by two groups (Miami and Oak Ridge), with excellent comparisons (no significant bias). Also the criteria for evaluating the quality of each run were initially derived independently by each group. It is thought that sensor and algorithm errors are no larger than in typical studies.

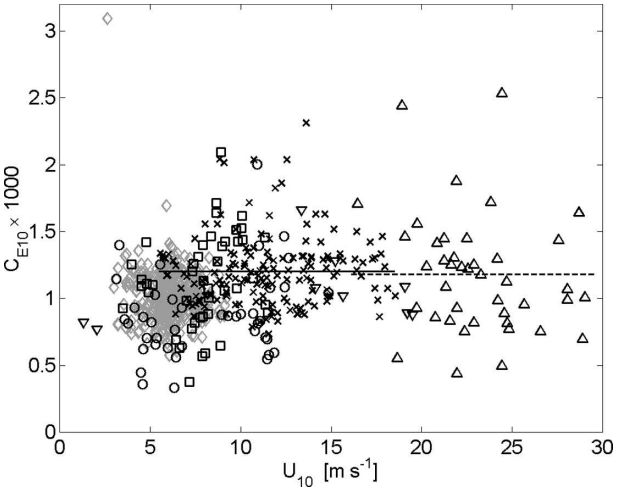

FIG. 11. Plot of Dalton number vs wind speed, both neutral 10 m. The CBLAST data points and mean value are shown with △ and dashed line, respectively. The HEXOS data (DeCosmo et al. 1996), shown with × and the solid line, have been corrected according to Fairall et al. (2003). Other symbols as in Fig. 2.

A possible source of bias is the lag time applied to w before correlating with q to obtain the flux. The selected time lag ($\varsigma = 0.20$ s for the BAT and $\varsigma_R = 0.30$ s for the Rosemount, with the 0.1-s difference between the two due to horizontal displacement of the two systems) is based on our best estimate for flow rates through the tubing plus the delay in internal LI-COR processing. To check the sensitivity of the calculated fluxes to ς, the fluxes were recalculated for different values of ς from 0 to 0.5 s. At the lower values, $\varsigma \approx 0 - 0.1$ s, the $w' - q'$ velocity cospectra exhibited negative contributions at high frequencies, contrary to what is expected from the universal cospectra (Kaimal et al. 1972). Based on these calculations, the estimated mean error in our flux estimates due to time lag effects ranges from −2.8% ($\varsigma = 0.15$) to +4.2% ($\varsigma = 0.3$), with no dependence on wind speed.

Mann and Lenschow (1994) and Mahrt (1998) discuss how short flight legs can yield systematic underestimates of covariance fluxes. This was a serious concern

among the authors, due to the limitations on flight leg length imposed by the operational need for clear air. As a result, all runs were thoroughly checked using ogive and cumulative sum analyses as discussed by French et al. (2007). Only runs passing these tests (thereby indicating that all low frequency scales are captured) were used in the analysis. Mahrt (1998) identified an additional error due to deviations of the aircraft from a constant altitude. During a typical CBLAST run, the average standard deviation about the nominal altitude was 7.8 m. The error results from what is essentially a Gaussian displacement distribution over a logarithmic mean humidity gradient. A thorough analysis of the problem by Mahrt et al. (2005) indicated this problem to be small, $O(1\%)$, except in very stable conditions.

Our use of SFMR winds for U_{10} is clearly a potential source of error. The SWEMODv2 algorithm, developed and validated using an extensive set of near-surface dropsonde winds, claims an accuracy of 2% at 30 m s^{-1}, or ± 1.5 m s^{-1} (Uhlhorn et al. 2007). A mean bias of 2% in U_{10N} would yield a similar bias in C_{E10N}. In contrast, the use of profile-derived winds instead of SFMR winds would yield a 5% reduction in Dalton number. We conservatively consider 5% as the uncertainty due to the surface winds.

The single largest potential source of bias appears to lie with the radiometric SSTs. The PRT-5 has a stated accuracy of $\pm 0.5°$, consistent with the corrections applied on N43RF by Burns et al. (2000) during TOGA COARE. A sensitivity analysis indicates that biases in SST of $[+1°, +0.5°, -0.5°, -1°\text{C}]$ would lead to biases in mean C_E of $[-24\%, -14\%, +19\%, +51\%]$, respectively. We are able to constrain the bias by plotting the measured surface heat flux (covariance of potential temperature Θ with vertical velocity) against the product $U_{10}(\Theta_0 - \Theta_{10})$ (not shown here), where Θ_0 is the SST. These plots indicate that, while we can rule out SST biases $O|0.5°|\text{C}$ or greater, a smaller bias is possible. Considering all factors, an uncertainty of $\pm 25\%$ in our mean Dalton number estimate seems to be a conservative estimate.

6. Discussion and conclusions

For some years now there has been considerable, and often heated, discussion on the effects of sea spray on heat transfer. There are now several spray models in the literature (e.g., Andreas and Emanuel 2001; Fairall et al. 1994; Makin 1998), each of which relies on assumptions about the size distribution (source function) of spray droplets and on how the droplets evaporate. The models assume the droplet number to increase with the whitecap or foam coverage of the sea surface, that is, either with $U^{3.4}$ (Monahan and Ó Muircheartaigh 1980) or u_*^3 (Wu 1979). Consequently the spray effect is expected to be significant only at high winds. For instance, Makin (1998) concludes that, although sea spray has negligible effects for wind speeds under 18 m s^{-1}, it should increase C_E by 20% for U = 30 m s^{-1}. Fairall et al. (1994) predict a near doubling of C_E due to spray effects by 20 m s^{-1}, with the Andreas and Emanuel (2001) prediction lying between the two.

It is evident that the CBLAST data do not support such an increase in Dalton number. In fact, the CBLAST data have either a small negative slope with wind speed, -0.03 ± 0.02 m s^{-1} (SFMR winds), or no significant dependence on it (profile winds). Andreas and DeCosmo (2002) argued that a sea spray effect was evident during HEXOS by comparing the HEXOS data to the C_E predictions of the then state-of-the-art Fairall et al. (1996) COARE-2.5 algorithm. Since the COARE-2.5 algorithm predicts a decrease in C_E with wind speed, Andreas and DeCosmo (2002) interpreted the lack of dependence of C_E with U in the HEXOS data as evidence of a sea spray effect. Although a similar argument could be made here, it should be pointed out that other algorithms (Zeng et al. 1998; COARE-3) predict a slight increase in C_E with wind speed—see Fig. 2. The argument of Andreas and DeCosmo (2002) does not hold when the Zeng or COARE-3.0 algorithms (neither of which incorporates spray physics) are used as the baseline.

That said, the CBLAST data do not rule out the possibility of a sea spray effect at higher wind speeds. Makin's (1998) prediction of a 20% sea spray effect at 30 m s^{-1} assumes a drag coefficient increasing linearly with wind speed, one similar to that of Large and Pond (1981) or Smith (1980). If, in fact, the drag coefficient levels off at the higher wind speeds (cf. Powell et al. 2003; Donelan et al. 2004; French et al. 2007), the spray production ($\propto u_*^3$) at high winds would be less, and the Makin prediction would be high. An effect of only $O(10\%)$ may well be obscured by uncertainties in the data.

The present CBLAST values of C_E and C_D (French et al. 2007) yield a C_E/C_D ratio of 0.69 ± 0.05 close to the Emanuel threshold of $C_E/C_D \approx C_K/C_D > 0.75$. In order for the threshold to be exceeded, some combination of increasing C_E and/or decreasing C_D must occur at wind speeds beyond the range of those measured here. Although the present results increase the wind speed range for humidity flux measurements by over 50%, flux data along with concurrent sea spray data are needed at even higher winds in order to fully understand the role of sea spray.

Acknowledgments. Support from ONR (N00014-01-F-0090) for CBLAST and from NOAA OAR (NA17-RJ-1226) for instrument development and further analysis is gratefully acknowledged. We appreciate the efforts of the many people involved in planning and carrying out CBLAST. We acknowledge in particular the efforts of Simon Chang and Carl Friehe (both formerly ONR), John Gaynor (NOAA OAR), Jim McFadden, Jim Roles, Terry Lynch, Barry Damiano, Ray Tong, and Richard McNamara at NOAA AOC and Frank Marks and Eric Uhlhorn (NOAA AOML). We also thank our CBLAST co-PIs as well the many scientists, engineers, and technicians at NOAA Aircraft Operations Center at MacDill AFB, Tampa, and NOAA AOML's Hurricane Research Division, along with the flight crew of N43RF.

REFERENCES

Andreas, E. L, and K. A. Emanuel, 2001: Effects of sea spray on tropical cyclone intensity. *J. Atmos. Sci.,* **58,** 3741–3751.

——, and J. DeCosmo, 2002: The signature of sea spray in the HEXOS turbulent heat flux data. *Bound.-Layer Meteor.,* **103,** 303–333.

Anthes, R. A., and S. Chang, 1978: Response of the hurricane boundary layer to changes of sea surface temperature in a numerical model. *J. Atmos. Sci.,* **35,** 1240–1255.

Banner, M. L., W. Chen, E. J. Walsh, J. B. Jensen, S. Lee, and C. Fandry, 1999: The Southern Ocean Waves Experiment. Part I: Overview and mean results. *J. Phys. Oceanogr.,* **29,** 2130–2145.

Black, P. G., and Coauthors, 2007: Air–sea exchange in hurricanes: Synthesis of observations from the Coupled Boundary Layer Air–Sea Transfer Experiment. *Bull. Amer. Meteor. Soc.,* **88,** 357–374.

Brutsaert, W., 1975: A theory for local evaporation (or heat transfer) from rough and smooth surfaces at ground level. *Water Resour. Res.,* **11,** 543–550.

Burns, S. P., and Coauthors, 2000: Comparisons of aircraft, ship, and buoy radiation and SST measurements from TOGA COARE. *J. Geophys. Res.,* **105,** 15 627–15 652.

Chen, S. S., J. F. Price, W. Zhao, M. A. Donelan, and E. J. Walsh, 2007: The CBLAST-Hurricane Program and the next-generation fully coupled atmosphere–wave–ocean models for hurricane research and prediction. *Bull. Amer. Meteor. Soc.,* **88,** 311–317.

DeCosmo, J., K. B. Katsaros, S. D. Smith, R. J. Anderson, W. A. Oost, K. Bumke, and H. Chadwick, 1996: Air–sea exchange of water vapor and sensible heat: The Humidity Exchange over the Sea (HEXOS) results. *J. Geophys. Res.,* **101,** 12 001–12 016.

Donelan, M. A., 1990: Air–sea interaction. *The Sea.* B. LeMéhauté and D. Hanes, Eds., Ocean Engineering Science, Vol. 9, John Wiley, 239–292.

——, and W. M. Drennan, 1995: Direct field measurements of the flux of carbon dioxide. *Air–Water Gas Transfer,* B. Jähne and E. C. Monahan, Eds., Aeon-Verlag, 677–683.

——, ——, and K. B. Katsaros, 1997: The air–sea momentum flux in conditions of wind sea and swell. *J. Phys. Oceanogr.,* **27,** 2087–2099.

——, B. K. Haus, N. Reul, W. J. Plant, M. Stiassnie, H. C. Graber, O. B. Brown, and E. S. Saltzman, 2004: On the limiting aerodynamic roughness of the ocean in very strong winds. *Geophys. Res. Lett.,* **31,** L18306, doi:10.1029/2004GL019460.

Drennan, W. M., and L. K. Shay, 2006: On the variability of the fluxes of momentum and sensible heat. *Bound.-Layer Meteor.,* **119,** 81–107.

——, K. K. Kahma, and M. A. Donelan, 1999: On momentum flux and velocity spectra over waves. *Bound.-Layer Meteor.,* **92,** 489–515.

——, H. C. Graber, D. Hauser, and C. Quentin, 2003: On the wave age dependence of wind stress over pure wind seas. *J. Geophys. Res.,* **108,** 8062, doi:10.1029/2000JC000715.

Emanuel, K. A., 1986: An air–sea interaction theory for tropical cyclones. Part I: Steady-state maintenance. *J. Atmos. Sci.,* **43,** 585–605.

——, 1995: Sensitivity of tropical cyclones to surface exchange coefficients and a revised steady-state model incorporating eye dynamics. *J. Atmos. Sci.,* **52,** 3969–3976.

Fairall, C. W., J. D. Kepert, and G. J. Holland, 1994: The effect of sea spray on surface energy transports over the ocean. *Global Atmos. Ocean Syst.,* **2,** 121–142.

——, E. F. Bradley, D. P. Rogers, J. B. Edson, and G. S. Young, 1996: Bulk parameterization of air–sea fluxes for TOGA COARE. *J. Geophys. Res.,* **101,** 3747–3764.

——, ——, J. E. Hare, A. A. Grachev, and J. B. Edson, 2003: Bulk parameterization of air–sea fluxes: Updates and verification for the COARE algorithm. *J. Climate,* **16,** 571–591.

Foster, R. C., 2005: Why rolls are prevalent in the hurricane boundary layer. *J. Atmos. Sci.,* **62,** 2647–2661.

French, J. R., W. M. Drennan, J. A. Zhang, and P. G. Black, 2007: Turbulent fluxes in the hurricane boundary layer. Part I: Momentum flux. *J. Atmos. Sci.,* **64,** 1089–1102.

Janssen, J. A. M., 1997: Does wind stress depend on sea state or not? A statistical error analysis of HEXMAX data. *Bound.-Layer Meteor.,* **83,** 479–503.

Johnson, H. K., J. Højstrup, H. J. Vested, and S. E. Larsen, 1998: On the dependence of sea surface roughness on wind waves. *J. Phys. Oceanogr.,* **28,** 1702–1716.

Kaimal, J. C., J. C. Wyngaard, Y. Izumi, and O. R. Coté, 1972: Spectral characteristics of surface-layer turbulence. *Quart. J. Roy. Meteor. Soc.,* **98,** 563–589.

Katsaros, K. B., M. A. Donelan, and W. M. Drennan, 1993: Flux measurements from a Swath ship in SWADE. *J. Mar. Syst.,* **4,** 117–132.

Kepert, J., 2001: The dynamics of boundary layer jets within the tropical cyclone core. Part I: Linear theory. *J. Atmos. Sci.,* **58,** 2469–2484.

Khelif, D., S. P. Burns, and C. A. Friehe, 1999: Improved wind measurements on research aircraft. *J. Atmos. Oceanic Technol.,* **16,** 860–875.

Kitaigorodskii, S. A., and Y. A. Volkov, 1965: On the roughness parameter of the sea surface and the calculation of momentum flux in the near-water layer of the atmosphere. *Izv. Atmos. Oceanic Phys.,* **1,** 973–988.

Kurihara, Y., and R. E. Tuleya, 1974: Structure of a tropical cyclone developed in a three-dimensional numerical simulation model. *J. Atmos. Sci.,* **31,** 893–919.

——, ——, and M. A. Bender, 1998: The GFDL hurricane prediction system and its performance in the 1995 hurricane season. *Mon. Wea. Rev.,* **126,** 1306–1322.

Large, W. G., and S. Pond, 1981: Open ocean momentum flux

measurements in moderate to strong winds. *J. Phys. Oceanogr.,* **11,** 324–336.

——, and ——, 1982: Sensible and latent heat flux measurements over the ocean. *J. Phys. Oceanogr.,* **12,** 464–482.

Liu, W. T., K. B. Katsaros, and J. A. Businger, 1979: Bulk parameterization of air–sea exchanges of heat and water vapor including the molecular constraints at the interface. *J. Atmos. Sci.,* **36,** 1722–1735.

Mahrt, L., 1998: Flux sampling errors from aircraft and towers. *J. Atmos. Oceanic Technol.,* **15,** 416–429.

——, D. Vickers, W. M. Drennan, H. C. Graber, and T. L. Crawford, 2005: Displacement measurement errors from moving platforms. *J. Atmos. Oceanic Technol.,* **22,** 860–868.

Makin, V. K., 1998: Air–sea exchange of heat in the presence of wind waves and spray. *J. Geophys. Res.,* **103,** 1137–1152.

Mann, J., and D. H. Lenschow, 1994: Errors in airborne flux measurements. *J. Geophys. Res.,* **99,** 14 519–14 526.

McGillis, W. R., and Coauthors, 2004: Air–sea CO2 exchange in the equatorial Pacific. *J. Geophys. Res.,* **109,** C08S02, doi:10.1029/2003JC002256.

Monahan, E. C., and I. Ó. Muircheartaigh, 1980: Optimal power-law description of oceanic whitecap coverage dependence on wind speed. *J. Phys. Oceanogr.,* **10,** 2094–2099.

Nicholls, S., and C. J. Readings, 1979: Aircraft observations of the structure on the lower boundary layer over the sea. *Quart. J. Roy. Meteor. Soc.,* **105,** 785–802.

Powell, M. D., P. J. Vickery, and T. A. Reinhold, 2003: Reduced drag coefficient for high wind speeds in tropical cyclones. *Nature,* **422,** 279–283.

Smith, S. D., 1980: Wind stress and heat flux over the ocean in gale force winds. *J. Phys. Oceanogr.,* **10,** 709–726.

——, and Coauthors, 1992: Sea surface wind stress and drag coefficients: The HEXOS results. *Bound.-Layer Meteor.,* **60,** 109–142.

Sreenivasan, K. R., A. J. Chambers, and R. A. Antonia, 1978: Accuracy of moments of velocity and scalar fluctuations in the atmospheric surface layer. *Bound.-Layer Meteor.,* **14,** 341–359.

Uhlhorn, E. W., and P. G. Black, 2003: Verification of remotely sensed sea surface winds in hurricanes. *J. Atmos. Oceanic Technol.,* **20,** 99–116.

——, ——, J. L. Franklin, M. Goodberlet, J. Carswell, and A. S. Goldstein, 2007: Hurricane surface wind measurements from an operational stepped frequency microwave radiometer. *Mon. Wea. Rev.,* in press.

Volkov, Y. A., 1970: Turbulent flux of momentum and heat in the atmospheric surface layer over a disturbed sea-surface. *Izv. Atmos. Oceanic Phys.,* **6,** 770–774.

Webb, E. K., G. I. Pearman, and R. Leuning, 1980: Correction of flux measurements for density effects due to heat and water vapour transfer. *Quart. J. Roy. Meteor. Soc.,* **106,** 85–100.

Wright, C. W., and Coauthors, 2001: Hurricane directional wave spectrum spatial variation in the open ocean. *J. Phys. Oceanogr.,* **31,** 2472–2488.

Wu, J., 1979: Oceanic whitecaps and sea state. *J. Phys. Oceanogr.,* **9,** 1064–1068.

Zeng, X., M. Zhao, and R. E. Dickinson, 1998: Intercomparison of bulk aerodynamic algorithms for the computation of sea surface fluxes using TOGA COARE and TAO data. *J. Climate,* **11,** 2628–2644.

Zhang, D., and R. A. Anthes, 1982: A high-resolution model of the planetary boundary layer—Sensitivity tests and comparisons with SESAME-79 data. *J. Appl. Meteor.,* **21,** 1594–1609.